



Brief paper

Computational tractable guaranteed numerical method to study the stability of n -dimensional time-independent nonlinear systems with bounded perturbation [☆]

Morgan Louedec ^{a,*}, Luc Jaulin ^a, Christophe Viel ^b

^a Lab-STICC, ENSTA-Bretagne, 2 rue François Verny 29200 Brest, France

^b CNRS, Lab-STICC, F-29806, Brest, France

ARTICLE INFO

Article history:

Received 6 July 2022

Received in revised form 14 December 2022

Accepted 20 January 2023

Available online xxxx

Keywords:

Stability

Positive invariance

Ellipsoid

Interval analysis

Numerical method

ABSTRACT

The stability analysis of nonlinear continuous systems often requires manual calculation, which can become time-consuming when dealing with complex systems. Some works use positive invariant sets to discuss stability. These sets can be numerically approximated using Interval analysis but the computational complexity is exponential. In this paper, we propose a computational tractable numerical but guaranteed method based on Interval analysis to verify the robust positive invariance of ellipsoids to automatize the study of n -dimensional nonlinear systems' stability. This method relies on a fast enclosure of a state integration by an Euler method. Interval analysis guarantees the results of the developed algorithms. Several examples show the effectiveness of the proposed approaches on n -dimensional non-asymptotical continuous systems subject to bounded perturbation.

© 2023 Elsevier Ltd. All rights reserved.

1. Introduction

The stability of dynamical systems can be studied with several methods. Classical methods consist in analytic calculations which may require a lot of time to be manually solved and may be specific to some problems. Thus, some numerical methods have been developed to automatically solve some stability problems, such as the Routh–Hurwitz criterion (Routh & Adams prize essay, 1877) or the Linear Matrix Inequalities (LMI) (Boyd, Ghaoui, Feron, & Balakrishnan, 1994). However, the class of problems currently solved by numerical methods is limited. There is therefore interest in developing new tools to automatize classical methods.

Lyapunov stability can be used to study the stability of nonlinear systems around an equilibrium point. The Lyapunov stability method consists in choosing a candidate Lyapunov function and then verifying if this candidate is positive-definite and decreases in time. This method involves manual calculation which becomes more challenging as the systems become more complex, see Qian, Li, Lee, and Ma (2018) and Zhou, Guo, Li, and Zhang (2019).

In these papers, the method is used several times with different Lyapunov functions. If the system is modified, a new Lyapunov function must be found and verified. Moreover, Lyapunov functions are more complex on a high-dimensional system with perturbations such as in Liu et al. (2018).

Some other works use positive invariant sets to discuss stability such as Blanchini and Miani (2015), Esterhuizen, Aschenbruck, and Streif (2020), Le Mezo, Jaulin, and Zerr (2017) and Valmorbida and Anderson (2017). These approaches are based on the links between the Lyapunov theory and the positive invariance concept since the sublevels sets of a Lyapunov functions are positive invariant. However, there exist invariant sets that are not related to any Lyapunov function. Ellipsoids are the most commonly exploited sets as candidate invariant regions because they can always be associated with a quadratic Lyapunov function.

Positive invariance of sets like ellipsoids can be verified under some criterion. For linear systems, they can be presented as LMI which can be numerically solved, see Lian and Wu (2020), Polyak, Nazin, Topunov, and Nazin (2006) and Weiss, Petersen, Baldwin, Erwin, and Kolmanovsky (2015). For nonlinear systems, they can be presented as inclusion problems as in Valmorbida and Anderson (2017) or as nonlinear inequality problems as in Romig, Jaulin, and Rauh (2019).

Interval analysis has been shown to provide efficient numerical approaches for solving various tasks in control theory, see Jaulin, Kieffer, Didrit, and Walter (2001), Rauh, Kersten, and Aschemann (2020) and Yu et al. (2020). Some interval analysis methods can be used to verify the positive invariance criterion

[☆] This work has been supported by the French Defence Innovation Agency (AID), France. The material in this paper was not presented at any conference. This paper was recommended for publication in revised form by Associate Editor Denis Efimov under the direction of Editor Luca Zaccarian.

* Corresponding author.

E-mail addresses: morgan.louedec@centraliens-nantes.org (M. Louedec), lucjaulin@gmail.com (L. Jaulin), christophe.viel@ensta-bretagne.fr (C. Viel).

for nonlinear systems in the presence of uncertainty. While the result of numerical methods is often non-guaranteed, numerical methods based on Interval calculation guarantee the verification of the criterion. The paper (Romig et al., 2019) approximates positive invariant sets using the Set Inversion Via Interval Analysis (SIVIA) presented in Jaulin et al. (2001). However, this method has exponential computational complexity, making it efficient for 2-dimensional problems but not suited for n -dimensional problems.

This paper proposes a new method to verify the robust positive invariance (RPI) of an ellipsoid for n -dimensional time-independent nonlinear continuous systems using interval analysis. To our knowledge, it is the first time that n -dimensional stability is studied with interval methods. The main idea of the method is to verify if the border of an ellipsoid, after one step of the Euler scheme, is still contained in the same ellipsoid to verify RPI via Nagumo's theorem. The result of the Euler scheme is outer approximated by another ellipsoid using Interval analysis. This method can be implemented to automatically verify the system's stability, so manual calculations can be avoided in the case of high dimensional problems. This numerical but guaranteed method has computational tractability, contrary to common numerical approaches like SIVIA (Romig et al., 2019) with exponential computational complexity.

The paper is structured in the following way. The key concept of ellipsoids, RPI, and interval analysis are presented in Section 2. Section 3 presents the positive invariance criterion which needs to be verified. The developed method is discussed in Section 4. Section 5 discusses the method with two case applications on 2-dimensional and n -dimensional nonlinear systems.

2. Notations and hypotheses

The theory of the numerical method presented in this paper relies on ellipsoids presented in Section 2.1, and on Interval analysis presented in Section 2.2. These mathematical tools will be used to prove the RPI presented in Section 2.3.

2.1. Ellipsoids

For a matrix $\mathbf{Q} \in \mathbb{R}^{n \times n}$, $\mathbf{Q} \succ 0$ means \mathbf{Q} is positive definite matrix, and $\mathbf{Q} \succeq 0$ means \mathbf{Q} is positive semi-definite. Let S_n^+ be the set of the real symmetric positive definite matrices.

Let us define the norm

$$\|\mathbf{x}\|_{\mathbf{Q}} = \sqrt{\mathbf{x}^T \mathbf{Q} \mathbf{x}}, \quad (1)$$

with $\mathbf{Q} \in S_n^+$. This norm can be associated with the scalar product

$$\langle \mathbf{x}, \mathbf{y} \rangle_{\mathbf{Q}} = \mathbf{x}^T \mathbf{Q} \mathbf{y}. \quad (2)$$

Let us define the *ellipsoid*

$$\mathcal{E}(\mathbf{Q}) = \{\mathbf{x} \in \mathbb{R}^n \mid \|\mathbf{x}\|_{\mathbf{Q}}^2 \leq 1\} \quad (3)$$

centred at the origin and described with $\mathbf{Q} \in S_n^+$.

For each $\mathbf{Q}_1 \in S_n^+$ and $\mathbf{Q}_2 \in S_n^+$, one has $\mathcal{E}(\mathbf{Q}_1) \subseteq \mathcal{E}(\mathbf{Q}_2)$ if and only if $\mathbf{Q}_1 - \mathbf{Q}_2 \succeq 0$.

The border of an ellipsoid $\mathcal{E}(\mathbf{Q})$ is written $\partial \mathcal{E}(\mathbf{Q})$. For each matrix $\mathbf{Q} \in S_n^+$, there exists a unique matrix $\Gamma_{\mathbf{Q}} \in S_n^+$ such that

$$\mathbf{Q} = \Gamma_{\mathbf{Q}}^{-1} \cdot \Gamma_{\mathbf{Q}}^{-1}, \quad (4)$$

with $\Gamma_{\mathbf{Q}} = (\sqrt{\mathbf{Q}})^{-1}$.

The numerical operations on the ellipsoid's matrix are guaranteed by interval analysis.

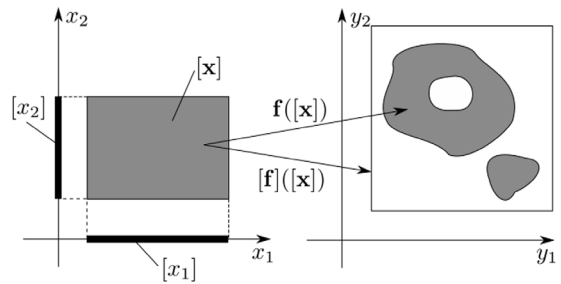


Fig. 1. Inclusion function in 2 dimension.

2.2. Interval analyses

Interval analysis is relevant to solve nonlinear inequalities in a guaranteed way. With basic mathematical tools, algorithms can be developed to test the conditions without further theory. This section presents interval analysis tools developed in Jaulin et al. (2001).

An *interval* $[x]$ is defined as a connected subset of \mathbb{R} . The set of intervals is written \mathbb{IR} . A *box* $[\mathbf{x}]$ is defined as a subset of \mathbb{R}^n and Cartesian product of intervals such that

$$[\mathbf{x}] = [x_1] \times [x_2] \times \dots \times [x_n]. \quad (5)$$

The set of boxes of \mathbb{R}^n is written \mathbb{IR}^n .

Definition 1. Let \mathbf{f} be a function from \mathbb{R}^n to \mathbb{R}^m . An *inclusion function* for \mathbf{f} is defined as an interval function $[\mathbf{f}]$ from \mathbb{IR}^n to \mathbb{IR}^m such that

$$\forall [\mathbf{x}] \in \mathbb{IR}^n, \mathbf{f}([\mathbf{x}]) \subset [\mathbf{f}]([\mathbf{x}]), \quad (6)$$

see Fig. 1.

Some inclusion functions give better approximation of $\mathbf{f}([\mathbf{x}])$. In this paper, the *centred inclusion functions* are the most suitable because ellipsoids are centred around the origin.

Definition 2. Let \mathbf{f} be a \mathcal{D}^1 function from \mathbb{R}^n to \mathbb{R}^m . The *centred inclusion function* for \mathbf{f} is an inclusion function defined as

$$[\mathbf{f}_c] : \mathbb{IR}^n \rightarrow \mathbb{IR}^m$$

$$[\mathbf{x}] \mapsto \mathbf{f}(\mathbf{x}_m) + \left[\frac{\partial \mathbf{f}}{\partial \mathbf{x}} \right]([\mathbf{x}])([\mathbf{x}] - \mathbf{x}_m) \quad (7)$$

with the middle point of $[\mathbf{x}]$ written \mathbf{x}_m .

2.3. Robust positive invariance

Consider the nonlinear systems

$$\dot{\mathbf{x}}(t) = \mathbf{f}(\mathbf{x}(t), \mathbf{w}(t)), \quad (8)$$

with the state $\mathbf{x}(t) \in \mathbb{R}^n$ and the bounded perturbation $\mathbf{w}(t) \in [\mathbf{w}] \subset \mathbb{R}^m$. Assume \mathbf{f} is \mathcal{D}^1 , and for each initial condition $\mathbf{x}(0)$ and piece-wise continuous function $\mathbf{w}(t)$ the system has a unique and globally defined solution.

Definition 3 (Blanchini and Miani (2015, Definition 4.3)). The set $S \subseteq \mathbb{R}^n$ is said to be *robust positive invariant* (RPI) with respect to (8) if, for all $\mathbf{x}(0) \in S$ and any $\mathbf{w}(t) \in [\mathbf{w}]$, the solution $\mathbf{x}(t)$ of system (8) is in S for all $t \geq 0$.

Fig. 2 presents an example of a RPI ellipsoid $\mathcal{E}(\mathbf{Q})$ on \mathbb{R}^2 . Section 3 presents a specific condition for RPI for Ellipsoids.

3. Problem formulation

This paper aims to discuss the stability of n -dimensional nonlinear system (8) around the origin. This stability is studied using RPI ellipsoids. The first step is to find an ellipsoid candidate for the system. Then the RPI of the ellipsoid is shown using a condition defined in this section. This condition will be tested by algorithmic approaches in the following sections.

Consider the nonlinear system described by (8) and the centred ellipsoid $\mathcal{E}(\mathbf{Q})$ with $\mathbf{Q} \in S_n^+$. A condition to verify the RPI of $\mathcal{E}(\mathbf{Q})$ is given using Nagumo's theorem. This condition is presented in Theorem 4.

Theorem 4 (Blanchini and Miani (2015, Section 4.4.1)). *The ellipsoid $\mathcal{E}(\mathbf{Q})$ is RPI w.r.t. (8) if and only if*

$$\forall \{\mathbf{x}, \mathbf{w}\} \in \partial\mathcal{E}(\mathbf{Q}) \times [\mathbf{w}], \langle \mathbf{x}, \mathbf{f}(\mathbf{x}, \mathbf{w}) \rangle_{\mathbf{Q}} \leq 0. \quad (9)$$

A numerical method to solve the stability problem is proposed in the following Section 4.

4. Enclosing method

We propose a new numerical method, called the enclosing method to verify the RPI, with operations on matrices of intervals. The method has computational tractability with a computational complexity between $O(n^2)$ and $O(n^3)$, as it will be illustrated in Fig. 6 in Section 5.2.2.

Let us define the function

$$\begin{aligned} \mathbf{h}_\delta : \mathbb{R}^{n+m} &\rightarrow \mathbb{R}^n \\ \{\mathbf{x}, \mathbf{w}\} &\mapsto \mathbf{x} + \delta \mathbf{f}(\mathbf{x}, \mathbf{w}), \end{aligned} \quad (10)$$

with an arbitrary small parameter $\delta > 0$. At a time $t > 0$, $\mathbf{h}_\delta(\mathbf{x}(t), \mathbf{w}(t))$ approximates the future state $\mathbf{x}(t + \delta)$, by the Euler method. Consider the set $\mathcal{Y}_\delta^{\mathbf{Q}}$ defined by

$$\mathcal{Y}_\delta^{\mathbf{Q}} = \{\mathbf{y} \in \mathbb{R}^n \mid \exists (\mathbf{x}, \mathbf{w}) \in \partial\mathcal{E}(\mathbf{Q}) \times [\mathbf{w}], \mathbf{y} = \mathbf{h}_\delta(\mathbf{x}, \mathbf{w})\}. \quad (11)$$

As shown in the following Theorem 5, if for all state $\mathbf{x}(t)$ on the border $\partial\mathcal{E}(\mathbf{Q})$ of an ellipsoid $\mathcal{E}(\mathbf{Q})$, the approximation of the future state $\mathbf{x}(t + \delta)$ is inside $\mathcal{E}(\mathbf{Q})$, then the state $\mathbf{x}(t)$ will stay inside $\mathcal{E}(\mathbf{Q})$, as illustrated by Fig. 2.

Theorem 5. *If there exists a $\delta > 0$ so that $\mathcal{Y}_\delta^{\mathbf{Q}} \subseteq \mathcal{E}(\mathbf{Q})$, then $\mathcal{E}(\mathbf{Q})$ is RPI w.r.t. (8).*

Proof. Assume $\mathcal{Y}_\delta^{\mathbf{Q}} \subseteq \mathcal{E}(\mathbf{Q})$. Let $\mathbf{x} \in \partial\mathcal{E}(\mathbf{Q})$ and $\mathbf{w} \in [\mathbf{w}]$. Since $\mathbf{h}_\delta(\mathbf{x}, \mathbf{w}) \in \mathcal{Y}_\delta^{\mathbf{Q}}$, one has $\mathbf{h}_\delta(\mathbf{x}, \mathbf{w}) \in \mathcal{E}(\mathbf{Q})$ and thus

$$\begin{aligned} \mathbf{h}_\delta(\mathbf{x}, \mathbf{w})^T \mathbf{Q} \mathbf{h}_\delta(\mathbf{x}, \mathbf{w}) &\leq 1 \\ \stackrel{(10)}{\Leftrightarrow} (\mathbf{x} + \delta \mathbf{f}(\mathbf{x}, \mathbf{w}))^T \mathbf{Q} (\mathbf{x} + \delta \mathbf{f}(\mathbf{x}, \mathbf{w})) &\leq 1 \\ \stackrel{(1), (8)}{\Leftrightarrow} \|\mathbf{x}\|_{\mathbf{Q}}^2 + 2\delta \mathbf{x}^T \mathbf{Q} \mathbf{f}(\mathbf{x}, \mathbf{w}) + \delta^2 \|\dot{\mathbf{x}}\|_{\mathbf{Q}}^2 &\leq 1 \\ \Leftrightarrow \|\mathbf{x}\|_{\mathbf{Q}}^2 + 2\delta \langle \mathbf{x}, \mathbf{f}(\mathbf{x}, \mathbf{w}) \rangle_{\mathbf{Q}} + \delta^2 \|\dot{\mathbf{x}}\|_{\mathbf{Q}}^2 &\leq 1 \\ \Leftrightarrow \langle \mathbf{x}, \mathbf{f}(\mathbf{x}, \mathbf{w}) \rangle_{\mathbf{Q}} \leq \frac{1}{2\delta} (1 - \|\mathbf{x}\|_{\mathbf{Q}}^2 - \delta^2 \|\dot{\mathbf{x}}\|_{\mathbf{Q}}^2). \end{aligned} \quad (12)$$

Moreover, since $\mathbf{x} \in \partial\mathcal{E}(\mathbf{Q})$, one has $\|\mathbf{x}\|_{\mathbf{Q}}^2 = 1$. Thus $\langle \mathbf{x}, \mathbf{f}(\mathbf{x}, \mathbf{w}) \rangle_{\mathbf{Q}} \leq 0$. Therefore, by Theorem 4, $\mathcal{E}(\mathbf{Q})$ is RPI. \square

In practice, the inclusion in Theorem 5 is hard to verify with a numerical method. Therefore, we propose to use instead an outer ellipsoidal approximation of $\mathcal{Y}_\delta^{\mathbf{Q}}$ to verify RPI as described in Corollary 6 of Theorem 5.

Corollary 6. *Let the ellipsoid $\mathcal{E}(\overline{\mathbf{Q}})$ be an outer approximation of $\mathcal{Y}_\delta^{\mathbf{Q}}$, i.e. $\mathcal{Y}_\delta^{\mathbf{Q}} \subseteq \mathcal{E}(\overline{\mathbf{Q}})$. If $\mathcal{E}(\overline{\mathbf{Q}}) \subseteq \mathcal{E}(\mathbf{Q})$ then $\mathcal{E}(\mathbf{Q})$ is RPI.*

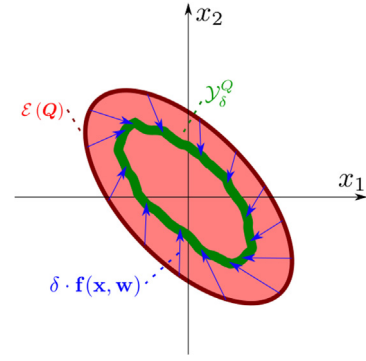


Fig. 2. RPI ellipsoid w.r.t. (8) with the Euler prediction of the function \mathbf{h}_δ with $\delta > 0$.

Note that $\mathcal{E}(\overline{\mathbf{Q}}) \subseteq \mathcal{E}(\mathbf{Q})$ is equivalent to $\overline{\mathbf{Q}} - \mathbf{Q} \geq 0$ which can be numerically verified with a Cholesky decomposition applied on interval matrix. The algorithm of this decomposition consists in using the interval counterpart of the operations in the classical Cholesky decomposition algorithm.

A method to find an outer ellipsoidal approximation $\mathcal{E}(\overline{\mathbf{Q}})$ is proposed in the next Section 4.1.

4.1. Outer ellipsoidal approximation

Inspired from Rauh and Jaulin (2021, Theorem 3), the outer ellipsoidal approximation $\mathcal{E}(\overline{\mathbf{Q}})$ can be calculated using the Theorem 7.

Theorem 7. *An outer ellipsoidal approximation of $\mathcal{Y}_\delta^{\mathbf{Q}}$ is $\mathcal{E}(\overline{\mathbf{Q}})$ with*

$$\overline{\mathbf{Q}} = \frac{1}{(1 + \rho)^2} \mathbf{A}_x^{-T} \mathbf{Q} \mathbf{A}_x^{-1} \quad (13)$$

where

$$\mathbf{A}_x = \frac{\partial \mathbf{h}_\delta}{\partial \mathbf{x}}(0, \mathbf{w}_m) \quad (14)$$

with \mathbf{w}_m as the middle of the box $[\mathbf{w}]$, and

$$\rho = \sup \{\|[\mathbf{b}]([\mathbf{x}], [\mathbf{w}])\|\} \quad (15)$$

with the tightest axis-aligned box $[\mathbf{x}]$ containing $\mathcal{E}(\mathbf{Q})$ and with the vector

$$\mathbf{b}(\mathbf{x}, \mathbf{w}) = \Gamma_{\mathbf{Q}}^{-1} \cdot \mathbf{A}_x^{-1} \cdot \mathbf{h}_\delta(\mathbf{x}, \mathbf{w}) - \Gamma_{\mathbf{Q}}^{-1} \cdot \mathbf{x} \quad (16)$$

Proof. Let $\mathbf{x} \in \partial\mathcal{E}(\mathbf{Q})$ and $\mathbf{w} \in [\mathbf{w}]$. Let us write $\mathbf{a}_1 = \Gamma_{\mathbf{Q}}^{-1} \cdot \mathbf{A}_x^{-1} \cdot \mathbf{h}_\delta(\mathbf{x}, \mathbf{w})$. From (16), one has

$$\mathbf{a}_1 = \Gamma_{\mathbf{Q}}^{-1} \cdot \mathbf{x} + \mathbf{b}(\mathbf{x}, \mathbf{w}) \quad (17)$$

Moreover, according to (3), (4), (15) and the triangular identity, one deduces

$$\begin{aligned} \|\mathbf{a}_1\| &\leq \left\| \Gamma_{\mathbf{Q}}^{-1} \cdot \mathbf{x} \right\| + \|\mathbf{b}(\mathbf{x}, \mathbf{w})\| \\ &\leq 1 + \rho. \end{aligned} \quad (18)$$

From (1), one has

$$\begin{aligned} &\|\mathbf{h}_\delta(\mathbf{x}, \mathbf{w})\|_{\overline{\mathbf{Q}}}^2 \\ &= \mathbf{h}_\delta(\mathbf{x}, \mathbf{w})^T \overline{\mathbf{Q}} \mathbf{h}_\delta(\mathbf{x}, \mathbf{w}) \\ \stackrel{(13)}{=} &\mathbf{h}_\delta(\mathbf{x}, \mathbf{w})^T \frac{1}{(1 + \rho)^2} \mathbf{A}_x^{-T} \mathbf{Q} \mathbf{A}_x^{-1} \mathbf{h}_\delta(\mathbf{x}, \mathbf{w}) \end{aligned}$$

$$\begin{aligned}
(4), (17) \quad & \frac{1}{(1+\rho)^2} \mathbf{a}_1^T \mathbf{a}_1 \\
& = \frac{1}{(1+\rho)^2} \|\mathbf{a}_1\|^2.
\end{aligned} \tag{19}$$

Therefore, with (18), one deduces that $\|\mathbf{h}_\delta(\mathbf{x}, \mathbf{w})\|_{\bar{\mathbf{Q}}} \leq 1$. As a result, $\mathbf{h}_\delta(\mathbf{x}, \mathbf{w}) \in \mathcal{E}(\bar{\mathbf{Q}})$ which verifies the theorem. \square

The parameter ρ can be calculated using the centred inclusion function for \mathbf{b} given by Theorem 8

Theorem 8. *The centred inclusion function for \mathbf{b} with the middle point $(\mathbf{x}, \mathbf{w}) = (0, 0)$ is equal to*

$$\begin{aligned}
& [\mathbf{b}]([\mathbf{x}], [\mathbf{w}]) \\
& = \mathbf{b}(0, \mathbf{w}_m) \\
& + \left(\Gamma_{\bar{\mathbf{Q}}}^{-1} \cdot \mathbf{A}_x^{-1} \left(\mathbf{I}_n + \delta \cdot \left[\frac{\partial \mathbf{f}}{\partial \mathbf{x}} \right]([\mathbf{x}], [\mathbf{w}]) \right) - \Gamma_{\bar{\mathbf{Q}}}^{-1} \right) \cdot [\mathbf{x}] \\
& + \Gamma_{\bar{\mathbf{Q}}}^{-1} \cdot \mathbf{A}_x^{-1} \cdot \delta \cdot \left[\frac{\partial \mathbf{f}}{\partial \mathbf{w}} \right]([\mathbf{x}], [\mathbf{w}]) \cdot ([\mathbf{w}] - \mathbf{w}_m).
\end{aligned} \tag{20}$$

Proof. From (7) the centred inclusion function for \mathbf{b} with the middle point $(0, 0)$ is

$$\begin{aligned}
& [\mathbf{b}]([\mathbf{x}], [\mathbf{w}]) \\
& = \mathbf{b}(0, \mathbf{w}_m) + \left[\frac{\partial \mathbf{b}}{\partial \mathbf{x}} \right]([\mathbf{x}], [\mathbf{w}]) \cdot ([\mathbf{x}] - 0) \\
& + \left[\frac{\partial \mathbf{b}}{\partial \mathbf{w}} \right]([\mathbf{x}], [\mathbf{w}]) \cdot ([\mathbf{w}] - \mathbf{w}_m) \\
& = \left[\frac{\partial \mathbf{b}}{\partial \mathbf{x}} \right]([\mathbf{x}], [\mathbf{w}]) \cdot [\mathbf{x}] + \left[\frac{\partial \mathbf{b}}{\partial \mathbf{w}} \right]([\mathbf{x}], [\mathbf{w}]) \cdot ([\mathbf{w}] - \mathbf{w}_m),
\end{aligned} \tag{21}$$

with the tightest axis-aligned box $[\mathbf{x}]$ containing $\mathcal{E}(\bar{\mathbf{Q}})$. The involved Jacobians are expressed as

$$\begin{aligned}
\frac{\partial \mathbf{b}}{\partial \mathbf{x}}(\mathbf{x}, \mathbf{w}) & = \Gamma_{\bar{\mathbf{Q}}}^{-1} \cdot \mathbf{A}_x^{-1} \frac{\partial \mathbf{h}_\delta}{\partial \mathbf{x}}(\mathbf{x}, \mathbf{w}) - \Gamma_{\bar{\mathbf{Q}}}^{-1} \\
& \stackrel{(10)}{=} \Gamma_{\bar{\mathbf{Q}}}^{-1} \cdot \mathbf{A}_x^{-1} \left(\mathbf{I}_n + \delta \cdot \left[\frac{\partial \mathbf{f}}{\partial \mathbf{x}} \right](\mathbf{x}, \mathbf{w}) \right) - \Gamma_{\bar{\mathbf{Q}}}^{-1}
\end{aligned} \tag{22}$$

$$\begin{aligned}
\frac{\partial \mathbf{b}}{\partial \mathbf{w}}(\mathbf{x}, \mathbf{w}) & = \Gamma_{\bar{\mathbf{Q}}}^{-1} \cdot \mathbf{A}_x^{-1} \cdot \frac{\partial \mathbf{h}_\delta}{\partial \mathbf{w}}(\mathbf{x}, \mathbf{w}) \\
& \stackrel{(10)}{=} \Gamma_{\bar{\mathbf{Q}}}^{-1} \cdot \mathbf{A}_x^{-1} \cdot \delta \cdot \left[\frac{\partial \mathbf{f}}{\partial \mathbf{w}} \right](\mathbf{x}, \mathbf{w}).
\end{aligned} \tag{23}$$

Moreover, the matrices \mathbf{A}_x and $\Gamma_{\bar{\mathbf{Q}}}$ do not depend on \mathbf{x} and \mathbf{w} , therefore the inclusion function of (22) and (23) can be deduced from the inclusion function of $\frac{\partial \mathbf{f}}{\partial \mathbf{x}}$ and $\frac{\partial \mathbf{f}}{\partial \mathbf{w}}$ such that

$$\begin{aligned}
\left[\frac{\partial \mathbf{b}}{\partial \mathbf{x}} \right]([\mathbf{x}], [\mathbf{w}]) & = \Gamma_{\bar{\mathbf{Q}}}^{-1} \cdot \mathbf{A}_x^{-1} (\mathbf{I}_n \\
& + \delta \cdot \left[\frac{\partial \mathbf{f}}{\partial \mathbf{x}} \right]([\mathbf{x}], [\mathbf{w}])) - \Gamma_{\bar{\mathbf{Q}}}^{-1},
\end{aligned} \tag{24}$$

$$\left[\frac{\partial \mathbf{b}}{\partial \mathbf{w}} \right]([\mathbf{x}], [\mathbf{w}]) = \Gamma_{\bar{\mathbf{Q}}}^{-1} \cdot \mathbf{A}_x^{-1} \cdot \delta \cdot \left[\frac{\partial \mathbf{f}}{\partial \mathbf{w}} \right]([\mathbf{x}], [\mathbf{w}]). \tag{25}$$

From (21), (24) and (25), one deduces (20). \square

The algorithmic application of Corollary 6 and Theorems 7 and 8 is presented in the following Section 4.2.

4.2. Algorithm of the enclosing method

The algorithm of the enclosing method is presented in Algorithm 1. This algorithm verifies if the ellipsoid $\mathcal{E}(\bar{\mathbf{Q}})$ is RPI w.r.t.

(8) with the perturbation $\mathbf{w} \in [\mathbf{w}]$. If the result is True, the ellipsoid is guaranteed RPI. If the result is False, the algorithm is not able to conclude.

The Algorithm depends on two sub-algorithms. The *enclose_ellipse_by_box* algorithm find the tightest axis-aligned box $[\mathbf{x}]$ such that $\mathcal{E}(\bar{\mathbf{Q}}) \subseteq [\mathbf{x}]$. The *is_definite_positive* algorithm return True if $\bar{\mathbf{Q}} - \mathbf{Q} \succ 0$ with a guaranteed method such as a Cholesky decomposition. It returns False if it is not able to conclude.

The two most complex operations in this algorithm are the matrix inversion and the Cholesky decomposition. Depending on their algorithm, these operations have a computational complexity between $O(n^2)$ and $O(n^3)$. Therefore the computational complexity of Algorithm 1 is expected to have a similar scale.

This algorithm will be applied to several examples in the following Section 5.

Algorithm 1 Algorithm of the enclosing method

Input $\bar{\mathbf{Q}}, \mathbf{f}, [\mathbf{w}], \delta$

Output res

- 1: $\Gamma_{\bar{\mathbf{Q}}} = (\sqrt{\bar{\mathbf{Q}}})^{-1}$
 - 2: $[\mathbf{x}] = \text{enclose_ellipse_by_box}(\bar{\mathbf{Q}})$
 - 3: $\mathbf{A}_x = \mathbf{I}_n + \delta \cdot \left[\frac{\partial \mathbf{f}}{\partial \mathbf{x}} \right](0, \mathbf{w}_m)$
 - 4: $[\mathbf{b}] = \mathbf{b}(0, \mathbf{w}_m) + \left(\Gamma_{\bar{\mathbf{Q}}}^{-1} \mathbf{A}_x^{-1} \right. \\ \left. \left(\mathbf{I}_n + \delta \cdot \left[\frac{\partial \mathbf{f}}{\partial \mathbf{x}} \right]([\mathbf{x}], [\mathbf{w}]) \right) - \Gamma_{\bar{\mathbf{Q}}}^{-1} \right) \cdot [\mathbf{x}] \\ \left. + \Gamma_{\bar{\mathbf{Q}}}^{-1} \cdot \mathbf{A}_x^{-1} \cdot \delta \cdot \left[\frac{\partial \mathbf{f}}{\partial \mathbf{w}} \right]([\mathbf{x}], [\mathbf{w}]) \cdot ([\mathbf{w}] - \mathbf{w}_m) \right)$
 - 5: $\|\mathbf{b}\| = \text{norm2}([\mathbf{b}])$
 - 6: $\rho = \text{upper_bound}(\|\mathbf{b}\|)$
 - 7: $\bar{\mathbf{Q}} = \frac{1}{(1+\rho)^2} \mathbf{A}_x^{-T} \bar{\mathbf{Q}} \mathbf{A}_x^{-1}$
 - 8: res = is_definite_positive($\bar{\mathbf{Q}} - \mathbf{Q}$)
-

5. Application

In this section, the RPI is tested with the enclosing method exposed in Section 4 on two example systems. The first example is a simple damping pendulum to illustrate the approaches with 2-dimensional ellipsoids. The second example is a n -dimensional nonlinear system, deduced from a platooning problem. Results are discussed in Section 5.3.

To find a good candidate for $\mathcal{E}(\bar{\mathbf{Q}})$, one may linearize the system at the equilibrium, then find a quadratic Lyapunov function with the Lyapunov equation (Blanchini & Miani, 2015, Section 4.4.1). Then, one may interpret this function as the norm (1), thus defining the matrix $\bar{\mathbf{Q}}$. In this case, $\mathcal{E}(\bar{\mathbf{Q}})$ is RPI w.r.t. the linearized system.

Note that RPI can also be verified by conventional procedures such as in Khalil (2001, Chapter 9) with Lyapunov function, or such as in Romig et al. (2019) with interval analysis. While there is plenty of result for the pendulum example such as in Hirsch, Smale, and Devaney (2013) and Khalil (2001), Lyapunov functions are more difficult to find for the 2nd example. Conventional interval analysis methods with bisection are relevant for the pendulum. But they are irrelevant to high dimensional problems because of the exponential computational time, as it will be shown in Fig. 6.

These tests are implemented in Python language with the libraries Codac for interval analysis, Scipy for symbolic expressions, Numpy for matrix operations, and Matplotlib for figure drawing. The code and further documentation is available at <https://morgan-louedec.fr/index.php/ellirpi/>

State trajectories illustrated by Figs. 3, 4(a) and 4(b) are simulated for 10 s with the Euler method with a time period $d_t = 0.1$ s.

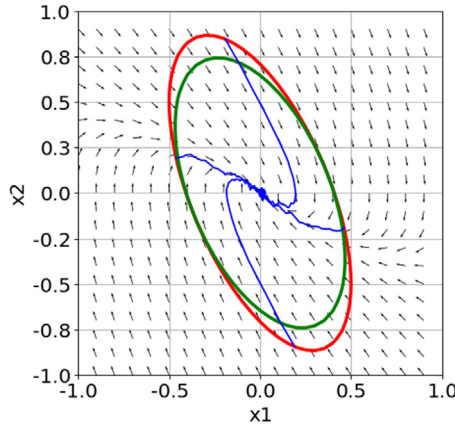


Fig. 3. Pendulum with the red ellipse $\partial\mathcal{E}(\mathbf{Q}_1)$, the green ellipse $\partial\mathcal{E}(\overline{\mathbf{Q}_1})$, the blue state trajectories starting on $\partial\mathcal{E}(\mathbf{Q}_1)$ and the black vector field $\mathbf{f}(\mathbf{x}, 0)$. (For interpretation of the references to color in this figure legend, the reader is referred to the web version of this article.)

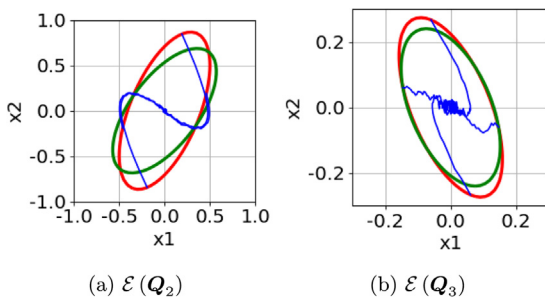


Fig. 4. Results for ellipsoids $\mathcal{E}(\mathbf{Q}_2)$ and $\mathcal{E}(\mathbf{Q}_3)$.

5.1. Pendulum

Consider a simple pendulum described by the state equations

$$\begin{cases} \dot{x}_1 = x_2 \\ \dot{x}_2 = -\sin(x_1) - 2 \cdot x_2 + w \end{cases} \quad (26)$$

where x_1 is the position of the pendulum, x_2 its rotational speed and w is a speed perturbation. Consider $[w] = [-0.1; 0.1]$.

5.1.1. Testing a positive invariant ellipsoid

The ellipsoid $\mathcal{E}(\mathbf{Q}_1)$ is tested with $\mathbf{Q}_1 = \begin{bmatrix} 6 & 2 \\ 2 & 2 \end{bmatrix}$ and the parameters $\delta = 0.1$. The Algorithm 1 verifies that $\mathcal{E}(\mathbf{Q}_1)$ is RPI. Fig. 3 illustrates the results.

One observes that the ellipsoid $\mathcal{E}(\overline{\mathbf{Q}_1})$ (in green) is inside the ellipsoid $\mathcal{E}(\mathbf{Q}_1)$ (in red). The matrix $\overline{\mathbf{Q}_1} - \mathbf{Q}_1$ has a Cholesky decomposition. Therefore $\overline{\mathbf{Q}_1} - \mathbf{Q}_1$ is positive definite. Thus, one can use Corollary 6 to show that $\mathcal{E}(\mathbf{Q}_1)$ is RPI. Indeed, one can observe that the four state trajectories starting on the ellipse $\partial\mathcal{E}(\mathbf{Q}_1)$ stay in the ellipsoid $\mathcal{E}(\mathbf{Q}_1)$ at any time and converge to a smaller set around origin.

5.1.2. Testing a non positive invariant ellipsoid

The ellipsoid $\mathcal{E}(\mathbf{Q}_2)$ is tested with $\mathbf{Q}_2 = \begin{bmatrix} 6 & -2 \\ -2 & 2 \end{bmatrix}$ and the parameters $\delta = 0.1$. The Algorithm 1 is not able to conclude. Fig. 4(a) illustrates the results.

One observes that $\mathcal{E}(\overline{\mathbf{Q}_2})$ is not inside $\mathcal{E}(\mathbf{Q}_2)$. Indeed, the Cholesky decomposition algorithm of $\overline{\mathbf{Q}_2} - \mathbf{Q}_2$ failed. Thus, the enclosing method cannot conclude on the robust positive invariance of $\mathcal{E}(\mathbf{Q}_2)$. One can also observe that some state trajectories starting on $\partial\mathcal{E}(\mathbf{Q}_2)$ exit $\mathcal{E}(\mathbf{Q}_2)$. \mathbf{Q}_2 is not RPI.

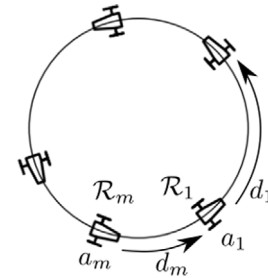


Fig. 5. Platooning on the circle.

5.1.3. Testing a small positive invariant ellipsoid

The ellipsoid $\mathcal{E}(\mathbf{Q}_3)$ is tested with $\mathbf{Q}_3 = 10\mathbf{Q}_1$ and the parameters $\delta = 0.1$. Note that $\mathcal{E}(\overline{\mathbf{Q}_3}) = \frac{1}{\sqrt{10}}\mathcal{E}(\mathbf{Q}_1)$ can be verified RPI with SIVIA methods. The Algorithm 1 is not able to conclude. Fig. 4(b) illustrates the results.

As in Section 5.1.2, the Cholesky decomposition of $\overline{\mathbf{Q}_3} - \mathbf{Q}_3$ failed. $\mathcal{E}(\overline{\mathbf{Q}_3})$ is not inside $\mathcal{E}(\mathbf{Q}_3)$ in Fig. 4(b). Therefore, the enclosing method cannot verify the positive invariance. Different values of δ were tested to find a better enclosing ellipsoid \mathbf{Q}_3 . Even with a very small value of δ , such as $\delta = 10^{-10}$, $\overline{\mathbf{Q}_3} - \mathbf{Q}_3$ is not verified positive definite.

5.2. n-Dimensional system

Consider m robots turning on a circular road of circumference L . Each robot \mathcal{R}_i with $i \in [1, \dots, m]$ satisfies the following state equation

$$\begin{cases} \dot{a}_i = v_i \\ \dot{v}_i = u_i + w_i \end{cases} \quad (27)$$

where a_i is the position of the robot, v_i its speed, u_i its control signal and w_i a small dynamical perturbation. Each robot \mathcal{R}_i is equipped with a radar that returns the distance d_i to the next robot \mathcal{R}_{i+1} and its derivative \dot{d}_i as illustrated by Fig. 5. The controller of \mathcal{R}_i is defined by

$$u_i = \arctan((d_i - d_d) + \dot{d}_i + (v_d - v_i)) \quad (28)$$

where $d_d = \frac{L}{m}$ is the desired value for d_i and where v_d is the desired value for v_i . The arctan(.) function illustrates a control saturation and makes the system non linear. Consider the state vector

$$\mathbf{x} = \begin{bmatrix} d_1 - d_d, d_2 - d_d, \dots, d_{m-1} - d_d, \\ v_1 - v_d, v_2 - v_d, \dots, v_m - v_d \end{bmatrix}^T \quad (29)$$

of dimension $n = 2m - 1$. This state is solution to the system

$$\dot{x}_i = \begin{cases} x_{m+i} - x_{m+i-1} & \text{for } i < m \\ \arctan(x_{i-m+1} + x_{i+1}) - 2x_i + w_{i-m+1} & \text{for } m \leq i < n \\ \arctan(x_m - 2x_n) - \sum_{k=1}^{m-1} x_k + w_m & \text{for } i = n \end{cases} \quad (30)$$

5.2.1. Example with 5 robots

Consider $[w_i] = [-10^{-4}; 10^4]$, $m = 5$ and $n = 2m - 1 = 9$. The 9-dimensional candidate ellipsoid $\mathcal{E}(\mathbf{Q}_n)$ is tested with the parameter $\delta = 0.01$, and \mathbf{Q}_n as the solution to the Lyapunov equation

$$\begin{aligned} \mathbf{A}^T \mathbf{Q}_n + \mathbf{Q}_n \mathbf{A} &= -10^j \mathbf{I}_n \\ \mathbf{A} &= \frac{\partial \mathbf{f}}{\partial \mathbf{x}}(0, 0) \end{aligned} \quad (31)$$

with $j = 4$. The Algorithm 1 verifies that $\mathcal{E}(\mathbf{Q}_n)$ is RPI.

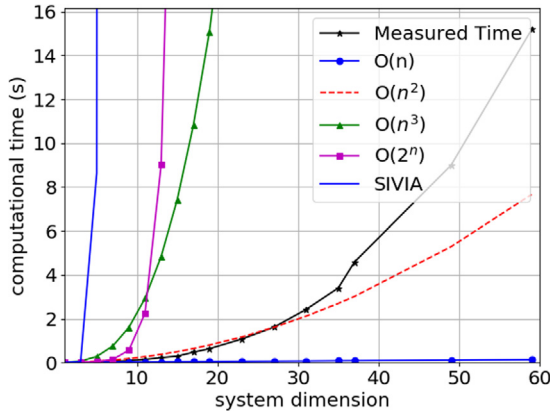


Fig. 6. Computational time.

5.2.2. Computational time with m robots

Different values of m are tested with $[w_i] = [-10^{-k}, 10^k]$, the perturbation amplitude $k > 0$, and \mathbf{Q}_n as the solution to (31). The parameters j , k and δ are adjusted to have $\mathcal{E}(\mathbf{Q}_n)$ verified RPI. In comparison, a SIVIA is also tested to solve (9). The computational time is measured and illustrated in Fig. 6. One can observe that the complexity of the enclosing algorithm is polynomial. In comparison, the computational time of the SIVIA method skyrockets. The SIVIA method is also limited by the random-access memory capacity which made it inoperative with $m > 3$ in the test.

5.3. Result and discussion

In the examples of the previous section, the enclosing methods verified the robust positive invariance of some candidates for the example systems.

Section 5.1.3 shows that the enclosing method has some pessimism and cannot always verify the RPI. It is only problematic with ellipsoids which are barely RPI. The method works better on systems whose linearization at the equilibrium is asymptotically stable. It is often the case for controlled systems.

Section 5.2 shows that the enclosing method is effective on high-dimensional systems. It is a big advantage compared to exponential solving methods such as the SIVIA method in Romig et al. (2019) which are inoperative on high dimensional problems.

The parameters δ can influence the chance of a conclusion. Thus, several attempts with different parameter values may be necessary.

Other ellipsoids verifying RPI can exist. Among them, the smallest RPI ellipsoid can approximate the zone where the state does not converge anymore. This smallest ellipsoid will be the subject of a future study. The methods could be generalized to time-dependent systems and time-dependent RPI ellipsoids. It will also be the subject of future study.

6. Conclusion

In this paper, a computational tractable method is presented to test the robust positive invariance of ellipsoids with respect to n -dimensional nonlinear systems with bounded perturbations. To our knowledge, it is the first time that n -dimensional stability is studied with interval methods. Ellipsoids allow for analysing the systems' stability around their equilibrium point. The developed method finds the image of the ellipsoid by a one-step Euler prediction, encapsulates this image with another ellipsoid, and uses it to verify the invariance criterion. This numerical method cannot always conclude on the positive invariance, but the invariance is guaranteed when a conclusion is found.

Future work will study the RPI of time-dependent ellipsoids. These ellipsoids will be used to solve problems with time-dependent systems or to find ellipsoidal state tubes. Moreover, the encompassing algorithm will be applied in the stability analysis of practical high-dimensional systems such as robot fleets. The calculation of the smallest RPI ellipsoid will also be investigated.

References

- Blanchini, Franco, & Miani, Stefano (2015). *Systems & control: Foundations & applications, Set-theoretic methods in control*. Cham: Springer International Publishing.
- Boyd, Stephen, Ghaoui, Laurent El, Feron, Eric, & Balakrishnan, Venkataraman (1994). *Linear matrix inequalities in system and control theory*. SIAM: Google-Books-ID: H2Nxxi5_fo0C.
- Esterhuizen, Willem, Aschenbruck, Tim, & Streif, Stefan (2020). On maximal robust positively invariant sets in constrained nonlinear systems. *Automatica*, 119, Article 109044.
- Hirsch, Morris W., Smale, Stephen, & Devaney, Robert L. (2013). *Differential equations, dynamical systems, and an introduction to chaos*. Elsevier.
- Jaulin, Luc, Kieffer, Michel, Didrit, Olivier, & Walter, Eric (2001). *Applied interval analysis*. London: Springer.
- Khalil, Hassan K. (2001). *Nonlinear systems* (3rd ed). Upper Saddle River, NJ: Pearson.
- Le Mezo, Thomas, Jaulin, Luc, & Zerr, Benoit (2017). An interval approach to compute invariant sets. *IEEE Transactions on Automatic Control*, 62(8), 4236–4242, Conference Name: IEEE Transactions on Automatic Control.
- Lian, Jie, & Wu, Feiyue (2020). Stabilization of switched linear systems subject to actuator saturation via invariant semiellipsoids. *IEEE Transactions on Automatic Control*, 65(10), 4332–4339, Conference Name: IEEE Transactions on Automatic Control.
- Liu, Yan-Jun, Lu, Shumin, Tong, Shaocheng, Chen, Xinkai, Chen, C. L. Philip, & Li, Dong-Juan (2018). Adaptive control-based Barrier Lyapunov Functions for a class of stochastic nonlinear systems with full state constraints. *Automatica*, 87, 83–93.
- Polyak, Boris T., Nazin, Alexander V., Topunov, Michael V., & Nazin, Sergey A. (2006). Rejection of bounded disturbances via invariant ellipsoids technique. In *Proceedings of the 45th IEEE conference on decision and control* (pp. 1429–1434). [ISSN: 0191-2216].
- Qian, Dianwei, Li, Chengdong, Lee, SukGyu, & Ma, Chao (2018). Robust formation maneuvers through sliding mode for multi-agent systems with uncertainties. *IEEE/CAA Journal of Automatica Sinica*, 5(1), 342–351, Conference Name: IEEE/CAA Journal of Automatica Sinica.
- Rauh, Andreas, & Jaulin, Luc (2021). A computationally inexpensive algorithm for determining outer and inner enclosures of nonlinear mappings of ellipsoidal domains. *International Journal of Applied Mathematics and Computer Science*, 31(3), 399–415.
- Rauh, Andreas, Kersten, Julia, & Aschemann, Harald (2020). Interval methods and contractor-based branch-and-bound procedures for verified parameter identification of quasi-linear cooperative system models. *Journal of Computational and Applied Mathematics*, 367, Article 112484.
- Romig, Swantje, Jaulin, Luc, & Rauh, Andreas (2019). Using interval analysis to compute the invariant set of a nonlinear closed-loop control system. *Algorithms*, 12(12), 262, Number: 12 Publisher: Multidisciplinary Digital Publishing Institute.
- Routh, Edward John, & Adams prize essay (1877). *A treatise on the stability of a given state of motion, particularly steady motion*. London, Macmillan and co.
- Valmorbida, Giorgio, & Anderson, James (2017). Region of attraction estimation using invariant sets and rational Lyapunov functions. *Automatica*, 75, 37–45.
- Weiss, Avishai, Petersen, Christopher, Baldwin, Morgan, Erwin, R. Scott, & Kolmanovskiy, Ilya (2015). Safe positively invariant sets for spacecraft obstacle avoidance. *Journal of Guidance, Control, and Dynamics*, 38(4), 720–732, Publisher: American Institute of Aeronautics and Astronautics _eprint: <https://doi.org/10.2514/1.G000115>.
- Yu, Dongmin, Mao, Yingying, Gu, Bing, Nojavan, Sayyad, Jermstittiparsert, Kittisak, & Nasser, Maryam (2020). A new LQG optimal control strategy applied on a hybrid wind turbine/solid oxide fuel cell/ in the presence of the interval uncertainties. *Sustainable Energy, Grids and Networks*, 21, Article 100296.
- Zhou, Jun, Guo, Yaohua, Li, Gongjun, & Zhang, Jun (2019). Event-triggered control for nonlinear uncertain second-order multi-agent formation with collision avoidance. *IEEE Access*, 7, 104489–104499, Conference Name: IEEE Access.



Morgan Louedec received a general engineering degree at the Ecole Centrale Nantes and a master of science in Electrical Engineering at the Technical University of Denmark in 2021. Since 2021, he is preparing for his Ph.D. at the LAB-STICC within the ENSTA Bretagne on the topic of the stability of groups of robots. His research interests are in the stability analysis of dynamical systems and guaranteed numerical tools.



Luc Jaulin was born in Nevers, France in 1967. He received the Ph.D. degree in automatic control from the University of Orsay, France in 1993 and the habilitation à Diriger des recherches degree in 2000. He is currently full Professor of Robotics at the ENSTA (Ecole Nationale Supérieure de Techniques Avancées) Bretagne, engineering school in Brest, France, since 2004. He does his research on underwater robotics using interval methods and constraint propagation in the ROBEX team (ROBotics for Exploration) of Lab-STICC. He is the co-author of more than 250 papers in

international journals and congress. He received the Moore in 2012 for his work on localization and map building of underwater robots using interval constraint propagation.



Christophe Viel received a master degree in “Advanced System and Robotic” and an engineering degree at the Arts et Metier ParisTech School in Paris (France) in 2014. He prepared his Ph.D. at the ONERA (The French Aerospace Lab) within the Paris-Saclay University on the topic “Determination of command control and observator for multi-agent system with reduced information by event-triggered” in 2017. After a first post-doctorate in 2018 at the University of Plymouth (UK) on control strategies for autonomous sailboat, and a second from 2019 to 2020 at the Institute of Science

of Movement in Marseille (France) on the topic of distance evaluations using optical flow, he is currently a CNRS researcher at the Lab-STICC on the topic of ROVs and the self-management of their umbilicals. His research interests are in distributed control and communication for multi-agent system, marine robotic, umbilical model and management.